Applied Catalysis B: Environmental 186 (2016) 1–9

Contents lists available at ScienceDirect

Applied Catalysis B: Environmental

journal homepage: www.elsevier.com/locate/apcatb

Methane steam reforming at low temperatures in a $BaZr_{0.7}Ce_{0.2}Y_{0.1}O_{2.9}$ proton conducting membrane reactor

V. Kyriakou[a,b], I. Garagounis[a,b], A. Vourros[a,b], E. Vasileiou[a,b], A. Manerbino[c], W.G. Coors[c], M. Stoukides[a,b,*]

[a] Department of Chemical Engineering, Aristotle University, Thessaloniki 54124, Greece
[b] Chemical Processes & Energy Resources Institute, CERTH, Thessaloniki 56071, Greece
[c] CoorsTek Inc., Golden, CO 80401, USA

ARTICLE INFO

Article history:
Received 14 September 2015
Received in revised form
12 December 2015
Accepted 18 December 2015
Available online 29 December 2015

Keywords:
Hydrogen production
Methane steam reforming
Ni-based catalyst
Membrane reactor
Proton conductors

ABSTRACT

The feasibility of Methane steam reforming (MSR) at low temperatures (450–650 °C) was studied in a Ni-BZCY72/BZCY72/Cu proton conducting membrane reactor, which allowed for the simultaneous separation of hydrogen. The cell reactor was first tested under open-circuit conditions, i.e., with the reactor operating as a catalytic reformer. The impact of several parameters, such as steam to carbon feed ratio, the operating temperature and the total flow rate was evaluated. The Ni-BZCY72 electrode exhibited high catalytic activity with methane conversion close to thermodynamic equilibrium, which was attributed to the high nickel content (45 wt.% after full reduction), as well as to the presence of ceria and zirconia in the support. Carbon dioxide was the main carbonaceous product with a molar ratio to carbon monoxide higher than 9, indicating that the Water Gas Shift reaction was predominant in the process. When hydrogen was electrochemically transported from the Ni-BZCY72 anode to the Cu cathode, a significant increase in methane conversion and hydrogen yield was observed. The methane conversion and hydrogen yield were improved by up to 50% in the temperature range of 550–650 °C over their corresponding open-circuit values. The BZCY72 perovskite exhibited satisfying proton fluxes and transference numbers at all temperatures and applied cell voltages examined. Finally, the Ni-BZCY72 reactor cell showed excellent chemical stability and durability, as well as coke tolerance for 24 h on stream.

1. Introduction

In the last few years, hydrogen has gained great interest as a future clean fuel for combustion engines or even fuel cells. The interest has increased significantly at the prospect of an emerging energy net, which will provide clean and viable energy solutions based on hydrogen and renewable sources. Thus, efficient production processes for hydrogen have been proposed and developed. These processes can be divided into three groups: (a) catalytic reforming of fossil fuels (natural gas accounts for more than 50% of the global production) (b) steam gasification of coal and (c) water electrolysis in alkaline solutions [1].

As the major component of natural gas methane is a compound of significant importance. Two factors, however, limit its use as a raw material. The first is that natural gas transportation is not economically advantageous and the second is that methane is a refractory molecule which complicates its conversion into upgraded products. Methane steam reforming (MSR) is the most efficient industrial technology for upgrading methane to useful products, such as hydrogen. MSR is a highly endothermic process in which Ni-based catalysts are employed to produce syngas, usually around a 1:3 of CO/H_2 ratio, at elevated temperatures (800–1000 °C). The dominant reactions are the highly endothermic reforming Reaction (1) and the slightly exothermic water gas shift (WGS) Reaction (2):

$$CH_4 + H_2O \rightarrow CO + 3H_2,\ \Delta H,_{298} = +206\,kJ/mol \quad (1)$$

$$CO + H_2O \rightarrow CO_2 + H_2,\ \Delta H,_{298} = -41\,kJ/mol \quad (2)$$

Syngas is a key-intermediate in the chemical industry and it is primarily used by ammonia and methanol manufacturers, as well as by refineries for hydrotreating [2]. In particular, the ammonia synthesis process requires high purity hydrogen derived through rather expensive separation procedures [1,3].

In the last few years, methane steam reforming at low temperatures (LT-MSR), i.e., between 400 and 650 °C, has been proposed to reduce the overall cost of the process [4,5]. Low temperatures

* Corresponding author at: Department of Chemical Engineering, Aristotle University, Thessaloniki 54124, Greece. Fax: +30 2310 996145.
E-mail address: stoukidi@cperi.certh.gr (M. Stoukides).

http://dx.doi.org/10.1016/j.apcatb.2015.12.039
0926-3373/

favor WGS and the dominant route of hydrogen production is the following:

$$CH_4 + 2H_2O \rightarrow CO_2 + 4H_2,\ \Delta H,_{298} = +165\ kJ/mol \quad (3)$$

The diminished energy demands and the cheaper reformer construction materials, due to lower operation temperatures, can lead to a significant reduction of the overall cost. Furthermore, the faster start-up and the absence of a WGS reactor are additional reasons that have made this idea attractive to many researchers [4,5]. However, despite the above advantages, at low temperatures methane conversion is suppressed by thermodynamic and kinetic limitations [6]. A possible solution to this problem is the use of catalytic membrane reactors (CMR) which allow continuous hydrogen removal and as a consequence an increase in methane conversion according to Le Chatelier's principle [5,7,8].

The CMR employs a selective Pd membrane with the reforming reactions and hydrogen separation taking place in a single stage [5,9,10]. The difference in hydrogen's chemical potential, which is enhanced by higher pressures in the reaction compartment, constitutes the driving force for hydrogen migration through the Pd membrane [5,9]. Complete methane conversion at 500–600 °C has been reported in these kind of systems, but in order to achieve it, high pressures that do not thermodynamically favor the MSR reaction were employed and the energy consumption increased [6]. Proton-conducting solid electrolytes have also been successfully tested as membranes for shifting the equilibrium of the MSR process, but usually as solid oxide fuel cells (SOFC) internal reformers operating at high temperatures of around 700–1000 °C [11–14]. In most of these cases, however, the primary aim was to generate electrical power and not to produce pure hydrogen [11–14].

Another interesting approach which is schematically represented in Fig. 1 is the use of a Solid Electrolyte Membrane Reactor (SEMR) for pure hydrogen production [15,16]. A gas mixture of methane saturated with steam is fed over the electro-catalyst (anode) where catalytic Reactions (1)–(3) take place. At closed-circuit conditions, with the use of an external power source, the produced hydrogen is converted into protons at the anode which are transported through the solid electrolyte to the cathode. At the cathode protons recombine with electrons and form molecular hydrogen which eventually evolves to the gas phase. This approach has the advantages of the CMR and at the same time, the employment of expensive Pd membranes and higher pressures is avoided. In the present communication, the MSR reaction was studied in a proton (H^+) conducting membrane reactor. The reactor consisted of a $BaZr_{0.7}Ce_{0.2}Y_{0.1}O_{2.9}$ (BZCY72) perovskite, which served as the proton conducting membrane, a tubular Ni-BZCY72 cermet, which served as the anodic electrode and a film of metallic Cu serving as the cathode. The anodic electro-catalyst is considered appropriate for this application because of its high Ni content and the presence of cerium and zirconium mixed oxides. The latter have been reported as very active supports [4,6]. The feasibility of LT-MSR in a SEMR at temperatures between 450 and 650 °C and under atmospheric pressure is examined, both catalytically and when hydrogen is electrochemically removed from the Ni-BZCY72 catalyst.

2. Experimental

2.1. Preparation and characterization of the proton conducting membrane reactor

The experimental apparatus used in the present study has been described in detail in a previous communication [17] and the schematic depiction of the reactor cell can be found therein. It was a slip-cast, electrode-supported tube, 20 cm long, with a diameter of nearly 1 cm and closed at one end, which was fabricated by CoorsTek Inc. (Golden, CO, USA). The cell was supported by its anode which was a porous two phase electrode (60 wt.% NiO–40 wt.% BZCY72) of an approximately 750 μm thickness and served as the working electrode. This high Ni content ensures not only a high conductivity of the cermet electrode but also, after the reduction of NiO to Ni, porosity which will facilitate gas diffusion to and from the three phase boundary (TPB). On the outer surface of this electrode a dense layer of BZCY72 with a thickness of 30 μm formed the electrolyte membrane of the cell [18]. A porous copper film was deposited on the outer surface of the BZCY72 electrolyte and served as the cathode (counter electrode). This electrode was prepared from a copper organometallic paste (Heraeus Precious Metals C7440 conductor paste). The paste was applied uniformly on the external surface of the tube near its closed end, over an area of 20 cm^2 followed by sintering at 1000 °C for 1 h under a 1 l min^{-1} flow of 4% hydrogen to argon.

The microstructure of the tube's surfaces was studied with TEM and SEM analyses. Preparation for the TEM analysis was accomplished with a FEI Helios NanoLab™ 600i DualBeam™ and was cleaned with 2 kV Ga beam. The image of the BZCY72 dense electrolyte was acquired using a 200 kV Philips CM200 transmission electron microscope. A Phenom ProX scanning electron microscope was used to acquire images of the cell cross sections, both polished and "as fractured" (with a diamond saw). X-ray diffractograms were obtained using a Bruker D8 Discover theta–theta diffractometer with a Cu Kα beam operating at 40 kV, 40 mA and a scan-rate o 0.3° in the 2θ range of 20°–80°. The patterns were obtained for both the BZCY72 electrolyte membrane and the Ni-BZCY72 cermet anode.

Temperature Programmed Oxidation (TPO) was used to examine the extent of carbon deposition at the anode. The Ni-BZCY72 anode was first exposed to a helium flow of 50 ml cm^{-3}, then the temperature was raised to 250 °C at a rate of 5 °C min^{-1} and was kept there for 1 h. This step was conducted to evaporate the adsorbed methane and water on the catalyst. Then, the reactor was heated to 800 °C under a flow of 5% oxygen in helium with a rate of 5 °C min^{-1}. The carbon dioxide and oxygen gasses were monitored continuously using a Binos infrared analyzer.

2.2. Reactant and product analysis

Reactant gas, methane and diluent nitrogen (Air Liquide Hellas) were certified standards of 99.95 or 5.2% and 99.999%, respectively. The steam feed was provided by bubbling the CH_4-N_2 mixture through a saturator. In order to prevent steam condensation the feed and exhaust tubes of the anode chamber were heated to at least 50 °C above the saturator's temperature. In the cathode chamber, a second stream of pure nitrogen was fed and served as a sweep gas for the hydrogen on that side. Analysis of reactants and products was performed by online gas chromatography. A SHIMADZU GC-14B chromatograph, equipped with a Molecular Sieve 5A column and nitrogen as the carrier gas, was used to measure the hydrogen concentration in the exhaust streams of both the outer (cathode) and the inner (anode) chamber. The carbon containing compounds (CH_4, CO, and CO_2) in the anode chamber exhaust stream, as well as methane concentration in the anode feed, were analyzed using a SHIMADZU GC-2014 chromatograph, which was equipped with a Porapak Q column and He as the carrier gas. The deviation in carbon balance did not exceed 3% indicating insignificant formation of carbon or other products.

All catalytic data were based on gas chromatograph measurements. In particular, conversion of reactants, selectivity and yield of products were calculated as follows.

$$CH_4\ \text{Conversion: } X_{CH_4} = \frac{F_{CH_4,in} - F_{CH_4,out}}{F_{CH_4,in}}\ [\%] \quad (4)$$

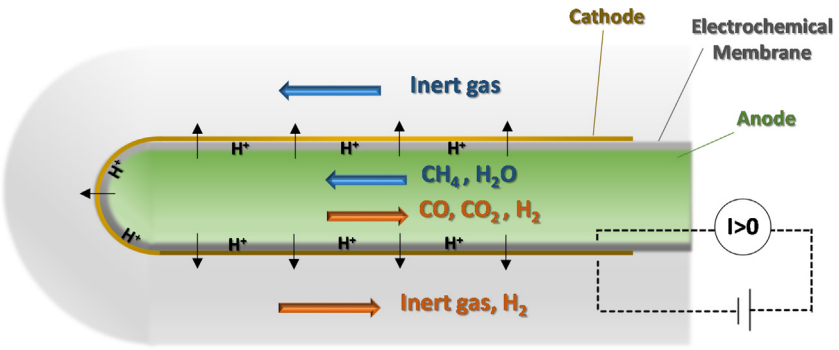

Fig. 1. Low-temperature methane steam reforming (LT-MSR) concept in a proton-conducting membrane reactor.

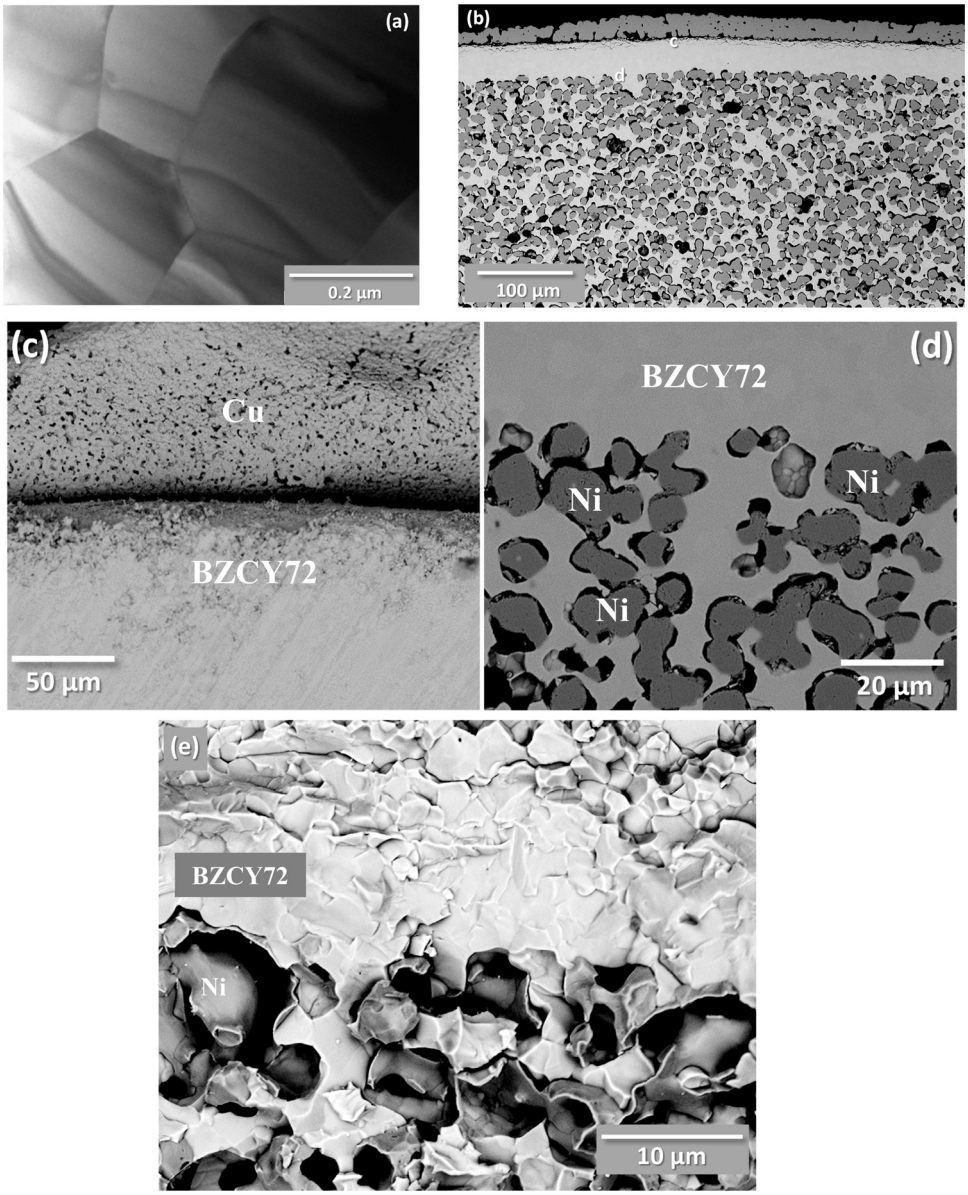

Fig. 2. (a) TEM image of the BZCY72 membrane surface and SEM images: (b) the polished cross-section of the cell, (c) the BZCY72/Cu interface, (d) "fresh" BZCY72/Ni-BZCY72 interface, (e) used BZCY72/Ni-BZCY72 interface. The NiO-BZCY72 was reduced under 4% H_2-96% Ar at 1000 °C for 24 h before exposure to reaction conditions.

$$\text{Product Selectivity: } S_j = \frac{F_j}{F_{CH_4,in} - F_{CH_4,out}} \times 100\,[\%] \quad (5)$$

$$\text{Hydrogen Yield: } Y_{H_2} = \frac{F_{H_2,anode} + F_{H_2,cathode}}{4 \times F_{CH_4,in}} \times 100\,[\%] \quad (6)$$

2.3. Electro-catalytic measurements

The potentiostatic operation for the closed circuit experiments was implemented by means of an AMEL 7050 galvanostat–potentiostat and the accompanying JuniorAssist 3.0.1 software. Silver wires were used as cell interconnects with the external circuit. When the cell operated under closed-circuit, three more dimensionless numbers were calculated in order to quantify the effect of hydrogen pumping on the reaction system. These are the proton transference number (PTN), the fraction of hydrogen separation (FSH) and the faradaic efficiency (FE). The PTN is the fraction of the developed current, I, that is carried by protons and can, therefore, be calculated by dividing the rate of hydrogen exiting the cathode chamber $r_{H_2,cathode}$, with the maximum rate of hydrogen that corresponds to the current I, as dictated by Faraday's law. Thus:

$$PTN = \frac{r_{H_2,cathode}}{\frac{I}{2} \times F} \quad (7)$$

where $F = 96485\,C\,mol^{-1}$ is Faraday's constant. The PTN of most materials depends strongly not only on temperature but also on the partial pressure of hydrogen and the presence of steam in the cell reactor. The PTN, t_{H+}, is necessary in the calculation of the FE, which is defined here as the ratio of the change in the reaction rate over the proton flux through the electrolyte. In the present case, FE is based upon the increase in carbon monoxide, $r_{elec,CO}$, and carbon dioxide, r_{elec,CO_2}, production. As the production of one molecule of carbon monoxide is accompanied by three molecules of hydrogen (Eq. (1)), while that of carbon dioxide (Eq. (3)) by four molecules of hydrogen (corresponding to six and eight protons, respectively), the FE can be calculated as follows:

$$FE = \frac{6 \times r_{elec,CO} + 8 \times r_{elec,CO_2}}{\frac{I \times t_{H+}}{F}} \quad (8)$$

The fraction of hydrogen separation is defined as the ratio of the hydrogen pumped to the cathode chamber to the total hydrogen production under closed-circuit conditions:

$$FSH = \frac{r_{H_2,cathode}}{r_{H_2,anode} + r_{H_2,cathode}} \quad (9)$$

where $r_{H_2,i}$ is the sum of the rates of hydrogen exiting the anode or cathode chambers, measured under steady state pumping.

3. Results and discussion

3.1. Characterization studies

A TEM image of the BZCY72 membrane after reduction appears in Fig. 2(a). The material is seen to be adequately dense with low residual porosity and clean grain boundaries. The microstructure of the cell's layers is also depicted in Fig. 2(b–e). The Cu film (counter electrode) exhibits low porosity as well as poor adhesion with the electrolyte. On the other hand the Ni-BZCY72 electrode appears to have not only good adhesion with the membrane but also a comparatively high porosity, which results from the reduction of the high NiO loading to metallic Ni. The average grain size of the Ni particles is less than 10 μm with a uniform distribution in the cermet layer. No significant agglomeration was observed after use, though none is expected for such low operation temperatures. The XRD patterns of the membrane and the anode can be observed in Fig. 3. The peaks of the BZCY72 phase are present in the diffractograms of both samples, while those of metallic Ni are clearly seen in the anode sample [19,20]. No other phase appears in either pattern confirming the lack of carbon (graphitic) deposition.

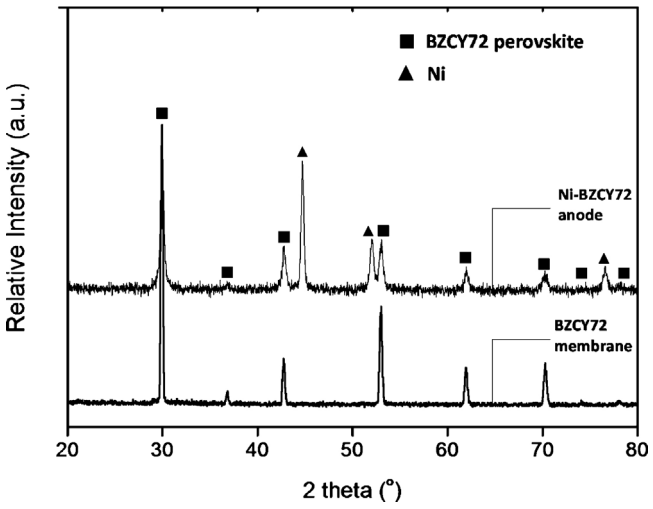

Fig. 3. XRD pattern of the BZCY72 membrane and Ni-BZCY72 anode. The membrane was ground off the anode after firing and reduction under 4% H_2 in Ar balance at 1000 °C for 24 h.

3.2. Catalytic performance assessment of Ni-BZCY72

The catalytic activity of the Ni-BZCY72 electrode was first evaluated for MSR at low temperatures under open-circuit conditions. These experiments are similar to experimental studies with a simple reforming reactor without employing any membrane technology. Fig. 4 shows the dependence of methane conversion and carbon dioxide selectivity on the total flowrate (Fig. 4a) and steam to carbon ratio (Fig. 4b) at 550 °C. In order to better evaluate the experimental data, the thermodynamic equilibrium conversion (dotted line) for the corresponding operating conditions is also plotted [6]. In Fig. 4a the steam/carbon (S/C) feed ratio was kept constant at 2 ($P_{CH_4} = 3$ kPa, $P_{H_2O} = 6$ kPa) and the flowrates varied from 15 to 120 $cm^{-3}\,min^{-1}$ equivalent to a space velocity (GHSV) of 300–2400 h^{-1}. It should be pointed out, however, that by taking into account the lower porosity of an electrode (Fig. 1) compared to a catalyst bed, the space velocity is underestimated. The open porosity of Ni-BZCY72 tubular electrodes has been measured at around 30% [21] leading to a GHSV of 1000–8000 h^{-1}. It can be seen from Fig. 4 that methane conversion is very close to that predicted from equilibrium at all flowrates examined, demonstrating the effectiveness of the Ni-BZCY72 catalyst. The carbon dioxide selectivity changes insignificantly above a flowrate of 30 $cm^{-3}\,min^{-1}$ and stabilizes around 95% indicating the extent of the WGS Reaction (2) at these operating conditions, with Reaction (3) as the overall reaction of the process. Fig. 4b depicts the influence of the S/C feed ratio on methane conversion and carbon dioxide selectivity. The total flowrate in the catalyst chamber was 30 $cm^{-3}\,min^{-1}$ (GHSV = 2000 h^{-1}) and the S/C ratio varied from 0.5–4 ($P_{CH_4} = 1.5$–12 kPa, $P_{H_2O} = 6$ kPa). The excess of steam ($S/C > 1$) benefits both methane conversion and carbon dioxide selectivity, which reached 55 and 97%, respectively, for $S/C = 4$. At low S/C feed ratios, the carbon dioxide selectivity decreases in favor of carbon monoxide. This occurs because the WGS reaction (Eq. (2)) which takes place as a second step is limited by the consumption of steam in the primary MSR reaction (Eq. (1)).

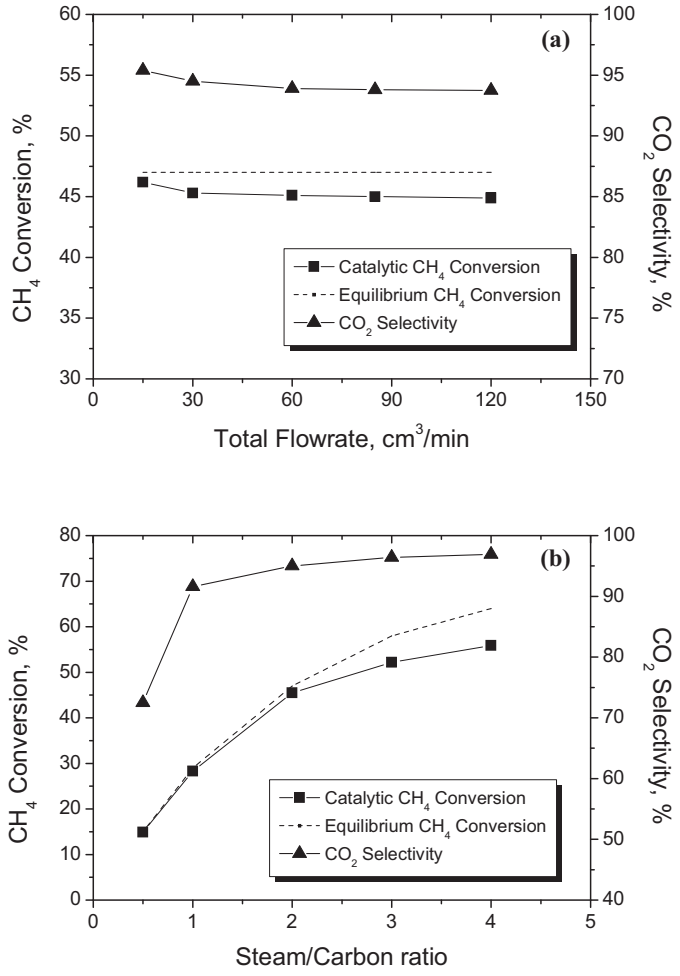

Fig. 4. Dependence of CH_4 conversion and CO_2 selectivity on total flowrate (a) and steam/carbon ratio (b) at 550 °C. (a) $S/C = 2$. (b) Ft = 30 cm^{-3} min^{-1}.

The choice of the anodic electro-catalyst is one of the key aspects for a LT-MSR process in a reactor cell to succeed. Materials that activate methane at low operating temperatures, have low tendency toward coke formation and at the same time show durability are needed [5]. The most common catalysts used in MSR are Ni-based, due to their high activity and lower cost than their noble metal-based counterparts [4,5,22–26]. As seen from Fig. 4, the Ni-BZCY72 catalyst exhibited excellent catalytic activity reaching conversions very close to thermodynamic equilibrium (especially at low S/C ratios) and over 90% selectivity to carbon dioxide proving its activity for the WGS reaction. This behavior of the electro-catalyst is not attributed only to Ni, but also to its interactions with its support.

The effect of the support on catalytic performance in LT-MSR is very important and has been studied in detail by many research groups [4]. In the present study the ceria and zirconia contained in BZCY72 have been applied as possible promoters for this reaction [5,19,27–31]. Matsumura and Nakamori [19]. studied silica, alumina and zirconia as possible supports of Ni for LT-MSR and found the latter as more active and resistant to oxidation [19]. Ceria is also a well-known support for reforming and oxidation reactions due to its excellent redox properties and durability under coke formation [4–6]. In addition, in some studies mixed ceria–zirconia oxide has been used either as is or as a promoter [27,28]. Despite the different materials and processes proposed, in all cases the use of zirconia and especially ceria has been reported to improve the activity and coke resistance of the catalyst during MSR and WGS [5,6,32].

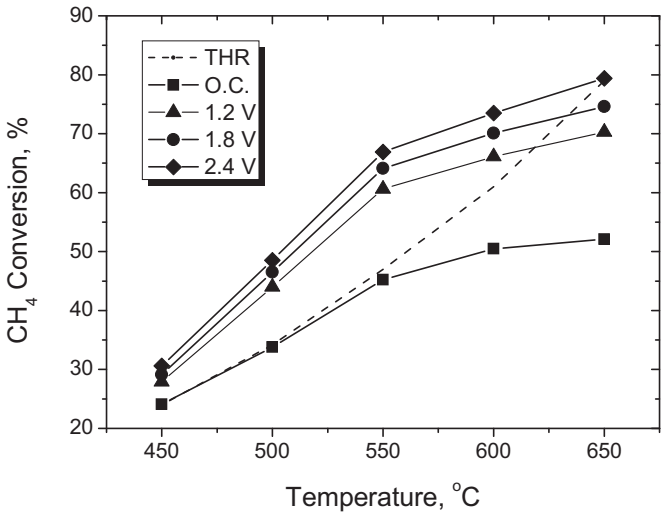

Fig. 5. Effect of temperature on the catalytic and electro-catalytic methane conversion. THR: Thermodynamic equilibrium, O.C.: open-circuit operation (catalytic). 1.2–2.4 V: proton conducting membrane operation at 1.2–2.4 V cell voltages. $S/C = 2$, Ft = 30 cm^{-3} min^{-1}.

3.3. Electrochemical membrane reactor operation

In the experiments carried out under closed-circuit conditions, pure nitrogen was introduced at the cathode side, while a mixture of methane and steam (P_{CH_4} = 3.0 kPa, P_{H_2O} = 6.0 kPa, $S/C = 2$) in nitrogen balance was fed to the Ni-BZCY72 anode side. Under these conditions, a steam to carbon ratio greater than 1.0, is sufficient to avoid coke formation [6]. So, in the closed-circuit experiments a constant value of two was used because it is the stoichiometric ratio of the desirable overall Reaction (3) and coke formation is prevented. The total pressure was atmospheric and the flowrates were 30 and 100 cm^{-3} min^{-1} for the anode and cathode chamber, respectively. Initially, the effect of temperature on the catalytic and electrocatalytic methane conversion over the Ni-BZCY72 electrode is examined and the results are shown in Fig. 5. The thermodynamic equilibrium conversion for these operating conditions is plotted again for comparison with an ideal reforming reactor. In the first place, it can be observed that the catalytic behavior of the Ni-BZCY72 electrode is close to thermodynamic equilibrium for temperatures up to 550 °C. By the application of positive cell voltages, i.e., when hydrogen was electrochemically removed from the catalyst, an impressive increase in methane conversion was observed at all temperatures tested. The results under proton pumping were obtained after a steady state open-circuit operation was first established. The electro-catalytic methane conversions per pass were higher than those of an equilibrium reformer without membrane in all cases except of 1.2 and 1.8 V at 650 °C. The difference in methane conversion between closed- and open-circuit operations increased with temperature and reached from 6.5 at 450 °C to 26.7% at 650 °C, for a 2.4 V cell voltage. At 550 °C the highest improvement in terms of methane conversion obtained was an impressive 49% increase from its initial catalytic value (reached 66.9 from 45.2% at 2.4 V). At 650 °C the improvement was slightly better at 50.5% but the conversion was only 0.4% higher than that of an equilibrium reactor. The beneficial effect of the applied voltage is attributed to the migration of produced hydrogen from the catalyst in the form of protons, which shifts the overall Reaction (3) towards the products according to Le Chatelier's principle.

Fig. 6 represents the dependence of hydrogen yield on cell voltage for temperatures between 450 and 650 °C. The yield of hydrogen is the rate of produced hydrogen in the reactor divided by the maximum amount of hydrogen that inlet methane could pro-

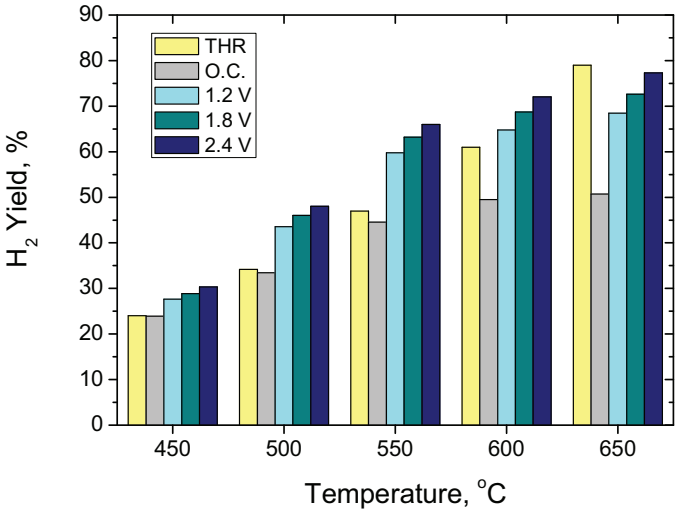

Fig. 6. Hydrogen yield obtained at catalytic (O.C.) and proton-conducting membrane (1.2–2.4 V) operation of the reactor cell at 450–650 °C. THR: Thermodynamic equilibrium, O.C.: open-circuit conditions (catalytic). 1.2–2.4 V: proton conducting membrane operation at 1.2–2.4 V cell voltages. $S/C = 2$, Ft = 30 cm^{-3} min^{-1}.

duce via Reaction (3) (Eq. (6)). The THR bar (yellow) represents the thermodynamic equilibrium value for hydrogen yield in an ideal reformer without membrane. It is also calculated by Eq. (6) assuming that the produced hydrogen is four times the reacted methane at equilibrium. The hydrogen yield increases significantly both with temperature and applied voltage and reached 77.9% at 650 °C and 2.4 V. At the same time the carbon dioxide selectivity took values higher than 90% and increased under closed-circuit conditions at the expense of carbon monoxide. Thus, it appears that WGS is also favored by hydrogen separation and the main route for hydrogen production is Reaction (3), which consequently favors the hydrogen yield. One can summarize the route for hydrogen production and separation in the cell as:

$$\text{Anode}: CH_4 + 2H_2O \rightarrow CO_2 + 8H^+ + 8e^- \quad (10)$$

$$\text{Cathode}: 8H^+ + 8e^- \rightarrow 4H_2 \quad (11)$$

Thus, the overall Reaction in the cell is the sum of (10) and (11), i.e., (3):

$$\text{Overall}: CH_4 + 2H_2O \rightarrow CO_2 + 4H_2 \quad (3)$$

It is not easy to compare the present results to those reported in the electrochemical membrane reactor literature. Research on this field focuses on electrical power generation at high temperatures (internal reforming SOFCs) either by partial oxidation or by dry or by steam reforming of methane without presenting detailed electro-catalytic data of MSR shifting [5,12,33–36]. Although, Hibino et al. investigated dry reforming of methane ($CH_4 + CO_2 \rightarrow 2CO + 2H_2$) in a $Ni/CaZr_{0.9}In_{0.1}O_{3-a}/Pt$ for hydrogen production and purification [35]. The process was studied at relatively high temperatures (750 °C) and stoichiometric ratio. The authors found that hydrogen pumping from the anode to the cathode at a current density of 24 mA cm^{-2} increased the methane conversion by around 33%. Most of the research work is focused on catalytic hydrogen membrane reactor either for mechanistic modeling or for experiments with variations in the design of reactors, the nature of catalysts and the space velocities [4,5]. However, in all of them both methane conversion and hydrogen yield increase by employing membrane technology, in fact, quite higher than those predicted from thermodynamic equilibrium (reaching even 100%). The above are in agreement with the present process where

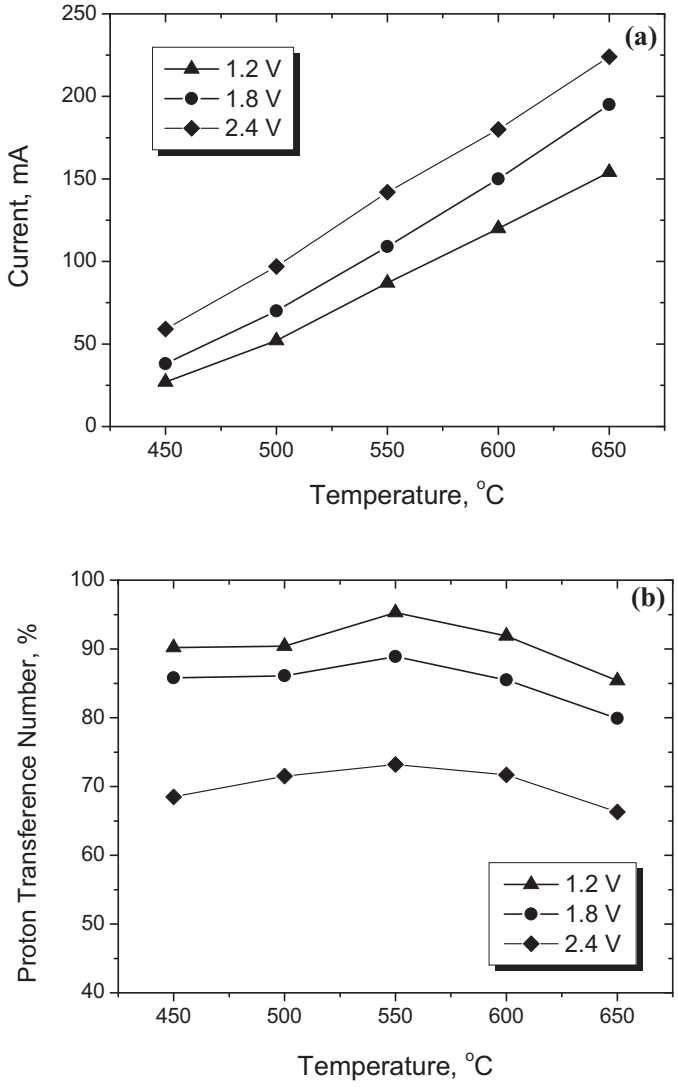

Fig. 7. Dependence of the developed current through the cell (a) and the PTN (b) on temperature. 1.2–2.4 V: proton conducting membrane operation at 1.2–2.4 V cell voltages. $S/C = 2$, Ft = 30 cm^{-3} min^{-1}.

hydrogen migration was beneficial for hydrogen production from methane.

The developed current and the PTN are crucial properties for a proton-conducting membrane's performance. Their variation with temperature at different applied voltages for the Ni-BZCY72/BZCY72/Cu cell is shown in Fig. 7. In Fig. 7a which contains results for current-voltage behavior, current increases with temperature, as expected, at all cell voltages. The current densities can be calculated easily by dividing the achieved currents with the 20 cm^2 superficial area of Cu cathode. They varied from 1.25 to 11.3 mA cm^{-2} between 1.2 V at 450 °C and 2.4 V at 650 °C, respectively. The PTN is defined as the fraction of the total current carried by protons in the cell and is calculated by Eq. (7) using electric and catalytic data. The protonic conductivity of the BZCY72 perovskite electrolyte may vary considerably, depending on many factors such as the temperature, the applied voltage and the gas composition each electrode is exposed to [37–40]. Fig. 7b shows the effect of temperature on the PTN for 1.2, 1.8 and 2.4 V cell voltages. The PTN was always at least 70%, due to the presence not only of hydrogen, but also of steam over the anode. Steam concentrations are essential for the proton transport mechanism in this kind of membranes

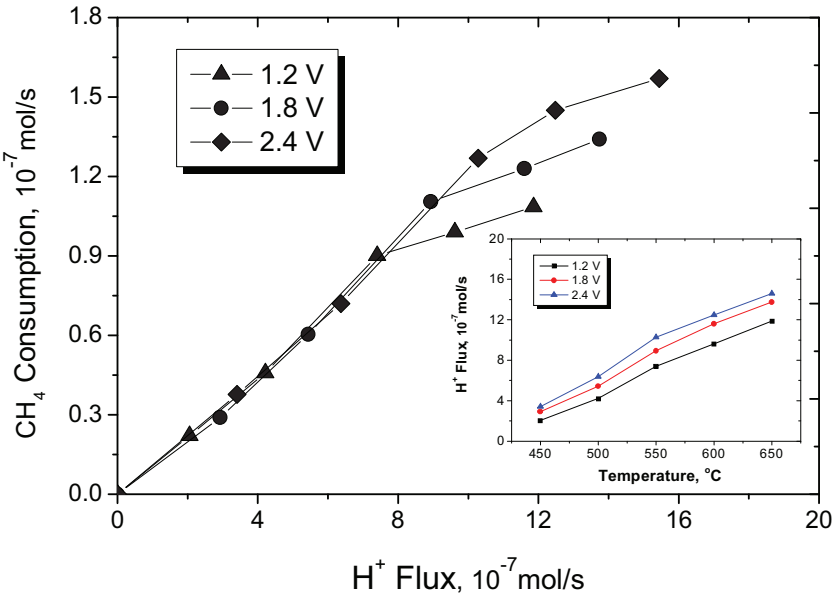

Fig. 8. Dependence of the net closed-circuit methane consumption rate on proton flux through the BZCY72 membrane. Inset: proton fluxes vs operating temperature at 1.2–2.4 V cell voltage. Proton conducting membrane operation at 1.2–2.4 V cell voltages. $S/C = 2$, Ft = 30 cm^{-3} min^{-1}.

[19,37–40] At 550 °C, the PTN in the present study exhibited a small maximum of 95.3, 88.9 and 73.2% at 1.2, 1.8 and 2.4 V, respectively.

The maxima in PTN are observed because the BZCY72 perovskite material at elevated temperatures (>600 °C) exhibits significant *p*-type conductivity at the expense of protons [39,40]. In addition, at 450 and 500 °C the low methane conversions at the anode lead to gas mixtures poorer in hydrogen, which also decreases proton conductivity, leading to the observed maximum at 550 °C. The drop in PTN with increasing voltage is most likely due to hydrogen depletion. In other words, higher voltages generate higher currents which leaves less hydrogen at the anode, making it harder for more protons to form. This is in agreement with the slightly greater difference in PTN observed at low temperatures where intrinsic H_2 production is lower. A possible future application of an LT-MSR process combined with proton-conducting membrane technology should employ materials which demonstrate pure protonic conductivity, in order to limit the cost of total electrical energy consumed. The BZCY72 perovskite exhibited proton conductivities up to 96% and seems to be close to these specifications. Furthermore, these materials are thought by many as ideal for such applications displaying satisfactory proton conductivities even in concentrated mixtures of steam and carbon dioxide [37,41].

Fig. 8 shows the effect of proton removal from the Ni-BZCY72 anode on the increase in methane consumption rate from open-circuit conditions. The proton flux through BZCY72 can be calculated by dividing the current carried by protons (I·PTN) with Faraday's constant ($F = 96485$ C mol^{-1}). The inset is provided in order to assist the reader in associating each value of proton flux (*x*-axis of the main Fig. 8) with operation temperature and cell voltage. A linear correlation of reacting methane under closed-circuit operation with removed protons is initially observed. At higher temperatures the correlation remains linear, but its slope decreases abruptly. This means that more protons need to be removed from the anode chamber for each new mole of methane to react. The Faradaic Efficiency (FE) is how many of the protons removed from the catalyst shift Reactions (1) or (3) (especially the latter) to the products side (Eq. (8)). If, for example, the only Reactions taking place in the cell are (10) and (11), an ideal 100% FE means that for every eight moles of protons removed from Ni-BZCY72, one new moles of methane reacts to form carbon dioxide. In the present study, FE followed a volcano type behavior with a peak at 550 °C with a maximum value of 88.3% at 1.8 V.

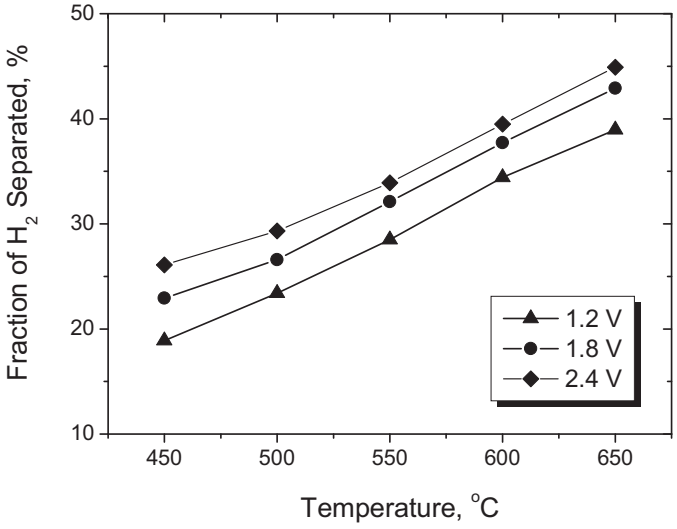

Fig. 9. Dependence of the fraction of hydrogen pumped to the cathode compartment (FSH) on temperature. Proton conducting membrane operation at 1.2–2.4 V cell voltages. $S/C = 2$, Ft = 30 cm^{-3} min^{-1}.

The effect of temperature on the FSH is shown in Fig. 9. FSH represents the fraction of the total amount of hydrogen formed in the reactor, which was electrochemically transported from the Ni-BZCY72 anode to the Cu cathode, in the form of protons through the solid electrolyte. In other words, it is the amount of produced hydrogen which was separated from the reaction mixture. The FSH increases almost linearly with temperature for all voltages applied and at 650 °C under 2.4 V reached 45%, which means that nearly half of the produced hydrogen was removed from the reaction mixture and obtained pure in the cathode compartment exhaust. However, these FSH values are relatively low and could be improved for a future application by changes in the reactor geometry. The reason for these low values is that the superficial area of the Cu cathode is smaller than that of the Ni-BZCY72 catalyst, which is the entire inner surface of the tube. In this way, hydrogen can only be

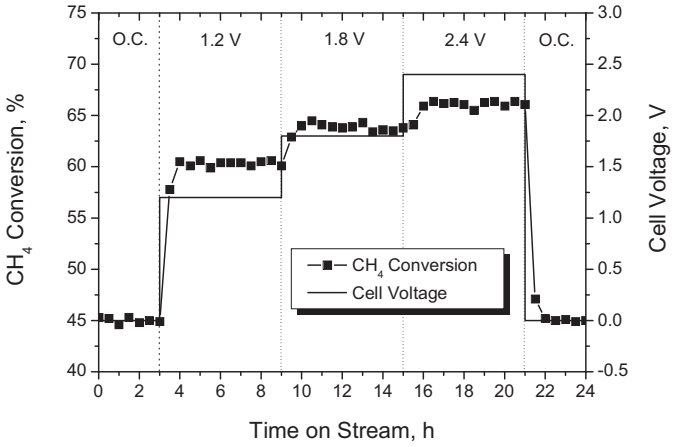

Fig. 10. Methane conversion variation during a short-term stability study under open- and closed-circuit conditions. Proton conducting membrane operation at 1.2–2.4 V cell voltages. $T = 550\,^{\circ}C$, $S/C = 2$, Ft = 30 cm^{-3} min^{-1}.

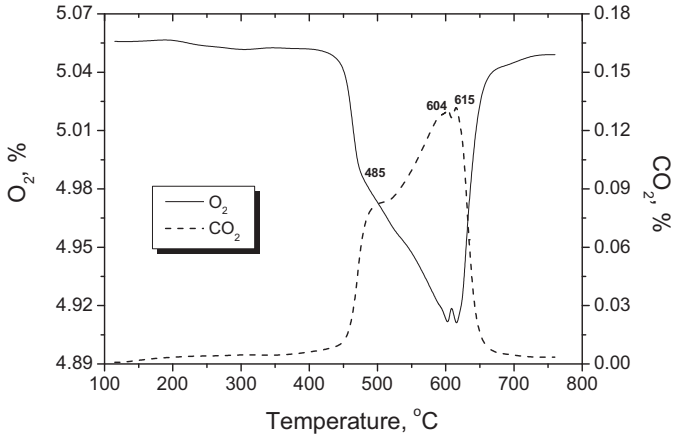

Fig. 11. TPO profile of the Ni-BZCY72 anode after 24 h step-change stability study.

removed from an area of the catalyst which approximately mirrors the Cu electrode on the inside of the tube and not from the whole of the active Ni-BZCY72 catalyst. In a previous work aiming at hydrogen separation from methane-steam mixtures where anodic and cathodic electrodes had matching superficial areas in a $SrZr_{0.95}Y_{0.05}O_{3-\alpha}$ proton conducting cell, FSH values as high as 95% were achieved [42].

In order to evaluate the durability of the cell, a 24 h stability test with step changes under open- and closed-circuit reaction conditions was carried out. The obtained methane conversion vs time on stream is plotted in Fig. 10. The operating temperature was 550 °C with a *S*/*C* ratio equal to 2.0, i.e., conditions with optimum performance in combined terms of FE, PTN and increase in methane conversion from the equilibrium value. Initially, the reactor was tested for 3 h under open-circuit conditions as a simple low temperature reformer. The conversion of methane was around 45% and very close to the equilibrium value of 47%, as shown in Fig. 5. Upon imposition of a 1.2 V constant voltage between anode and cathode the conversion of methane increased rapidly to 60% and stayed close to this value for 6 h. Next the imposed voltage was changed to 1.8 V and as a consequence methane conversion increased to 64% revealing an excellent behavior for another 6 h. The same behavior was observed when the voltage reached 2.4 V, but this time conversion was 67%. Finally, by opening the circuit the conversion returned quickly to its initial value without any obvious degradation. One can realize from Fig. 10 that the present configuration allows in situ control of methane conversion and consequently hydrogen yield, by a simple alteration of the cell voltage through an external power source.

The above stability test was followed by Temperature Programmed Oxidation (TPO) in order to identify carbon deposited on Ni-BZCY72. The results are shown in Fig. 11. Three carbon dioxide peaks at 485, 604 and 615 °C were observed, accompanied by simultaneous oxygen consumption. The peak at 485 °C indicates the existence of reactive amorphous carbon species on the surface of nickel, such as CH*x* (*x* = 1,2,3), which can be eliminated easily at low temperatures [43,44]. The two peaks at 604 and 615 °C are ascribed to the oxidation of more inert carbon species in the form of graphite [43,44].

Efforts regarding the chemical stability of barium-cerate (BCY) proton conducting materials under concentrated hydrocarbon, carbon dioxide or monoxide and steam concentrations have been made in recent years [20,37,40,41,45]. Among these the high doping in zirconia, as in the perovskite employed in the present study, have been proved as the best trade-off solution between stability and proton conductivity [37,40]. Fang et al. [20]. showed that BZCY72 perovskites suffer degradation and loss in hydrogen permeability at high temperatures (850–950 °C) especially due to the formation of barium carbonate and nickel corrosion from carbon monoxide. However, at milder operating conditions and for $x > 0.3$ in $BaZr_xCe_{1-x}Y_{0.1}O_{3-\delta}$ perovskites, as in this work, the membrane exhibited outstanding stability without any sign of barium carbonate formation [37,41,45]. Moreover, the corrosion of nickel is suppressed due to the low carbon monoxide concentrations.

The 24 h stability study indicates suitable activity and stability under the explored reaction conditions (Figs. 10 and 11). However, in any scale-up attempt where higher feed concentrations or flowrates are used possible coke formation could partially deactivate the anode. A possible solution to this problem has been demonstrated by de Lucas-Consuegra et al. [46], who studied hydrogen production from methane in a single compartment configuration employing Na-βAl_2O_3 as solid electrolyte and Pt-YSZ as working electrode. They proved that deactivated platinum electrodes could be regenerated by simply imposing a negative polarization which enhanced the coverage in oxygen or steam species [46]. Similarly, the present system offers the possibility to in situ regenerate the catalyst by a short term reversal of polarization. The latter demonstrates further the high potential for scale-up and development of a proton-conducting membrane reactor for LT-SMR. Nevertheless, further research work with long-term experiments should be done to clarify the limits of stable performance of the proposed process.

4. Conclusions

Methane steam reforming at low temperatures (LT-MSR) was experimentally investigated in a Ni-BZCY72/BZCY72/Cu proton conducting membrane reactor which allowed the separation of hydrogen. The cell reactor was first tested under open-circuit conditions (catalytic reformer operation) and the effect of steam to carbon (*S*/*C*) ratio and total flowrate was evaluated in the temperature range of 450–650 °C. The Ni-BZCY72 electrode was found to be highly active with methane conversions close to equilibrium, especially when low S/C ratios were employed (<2). The high selectivities to carbon dioxide (around 95%) indicate that WGS (Eq. (2)) was nearly as extensive as MSR (Eq. (1)) making Eq. (3) the main route for hydrogen production.

Upon closing the circuit and electrochemically removing hydrogen from the Ni-BZCY72 catalyst, a considerable increase in methane conversion and consequently to hydrogen yield was observed. Specifically, methane conversion reached 80% (77% hydrogen yield) at 650 °C under 2.4 V corresponding to an improve-

ment from the initial value under open-circuit of 50%. The maximum hydrogen separation from the reaction mixture was rather low and close to 45%, a result which was attributed to the difference between the anodic and cathodic electrode areas. The PTN of the BZCY72 perovskite took values between 67 and 95% and exhibited a strong dependence on gas concentration, temperature and applied cell voltage. Furthermore, the Ni-BZCY72 reactor cell showed excellent chemical stability and durability, as well as coke tolerance in a short-term 24 h test with variation of the cell voltage. Despite the encouraging results presented herein more detailed studies focused on these materials' behavior should be conducted before scale-up can be attempted.

Acknowledgements

The authors would like to thank Dr. Brian Gorman and Dr. David Diercks at the Colorado School of Mines for their help in acquiring the TEM image.

References

[1] S.A. Ritter, A.D. Ebner, Sep. Sci. Technol. 42 (2007) 1123–1193.
[2] J.R. Rostrup-Nielsen, J. Sehested, J.K. Norskov, Adv. Catal. 47 (2002) 65–139.
[3] A.B. Shigarov, V.D. Meshcheryakov, V.A. Kirillov, Theor. Found. Chem. Eng. 45 (2011) 595–609.
[4] S.D. Angeli, G. Monteleone, A. Giaconia, A.A. Lemonidou, Int. J. Hydrogen Energy 39 (2014) 1979–1997.
[5] R. Chaubey, S. Sahu, O.O. James, S. Maity, Renew. Sustain. Energy Rev. 23 (2013) 443–462.
[6] Z.W. Liu, K.W. Jun, H.S. Roh, S.E. Park, J. Power Sources 111 (2002) 283–287.
[7] D.S.A. Simakov, M. Sheintuch, Ind. Eng. Chem. Res. 49 (2010) 1123–1129.
[8] S. Wieland, I.T. Melin, I.A. Lamm, Chem. Eng. Sci. 57 (2002) 1571–1576.
[9] J. Tong, Y. Matsumura, Catal. Today 111 (2006) 147–152.
[10] E. Kikuchi, Catal. Today 25 (1995) 333–337.
[11] M. Andersson, H. Paradis, J. Yuan, B. Sunde'n, Int. J. Energy Res. 35 (2011) 1340–1350.
[12] H. Iwahara, H. Uchida, K. Morimoto, S. Hosogi, J. Appl. Electrochem. 19 (1989) 448–452.
[13] G.W. Coors, J. Electrochem. Soc. 151 (2004) A994–A997.
[14] G.W. Coors, J. Power Sources 118 (2003) 150–156.
[15] C. Kokkofitis, M. Ouzounidou, A. Skodra, M. Stoukides, Solid State Ionics 178 (2007) 507–513.
[16] S. Yamaguchi, S. Yamamoto, B. Tsuchiya, S. Nagata, T. Shishido, J. Power Sources 145 (2005) 712–715.
[17] E. Vasileiou, V. Kyriakou, I. Garagounis, A. Vourros, A. Manerbino, G.W. Coors, M. Stoukides, Top. Catal. 58 (2015) 1193–1201.
[18] W.G. Coors, Advances in Ceramics—Synthesis and Characterization, Processing and Specific Applications, in: C. Sikalidis (Ed.), InTech, 2011, pp. 479–500.
[19] Y. Matsumura, T. Nakamori, Appl. Catal. A: Gen. 258 (2004) 107–114.
[20] S. Fang, K.S. Brinkman, F. Chen, J. Membr. Sci. 467 (2014) 85–92.
[21] G.W. Coors, J. Membr. Sci. 458 (2014) 245–253.
[22] A. Dicks, K. Pointon, A. Siddle, J. Power Sources 86 (2000) 523–530.
[23] S. Bebelis, A. Zeritis, C. Tiropani, S. Neophytides, Ind. Eng. Chem. Res. 39 (2000) 4920–4927.
[24] J. Meusinger, E. Riensche, U. Stimming, J. Power Sources 71 (1998) 315–320.
[25] H. Timmermann, W. Sawady, R. Reimert, E. Ivers-Tiffee, J. Power Sources 195 (2010) 214–222.
[26] G. Jones, J.G. Jakobsen, S.S. Shim, J. Kleis, M.P. Andersson, J. Rossmeisl, F. Abild-Pedersen, T. Bligaard, S. Helveg, B. Hinnermann, J. Catal. 259 (2008) 147–160.
[27] A. Kambolis, H. Matralis, A. Trovarelli, C. Papadopoulou, Appl. Catal. A: Gen. 377 (2010) 16–26.
[28] M.H. Halabi, M.H.J.M. Croon, J. van der Schaaf, P.D. Cobden, J.C. Schouten, Appl. Catal. A: Gen. 389 (2010) 68–79.
[29] L. Marra, P.F. Wolbers, F. Gallucci, M. van Sint Annaland, Catal. Today 236 (2014) 23–33.
[30] G. Postole, T.S. Nguyen, M. Aouine, P. Gélin, L. Cardenas, L. Piccolo, Appl. Catal. B: Environ. 166–167 (2015) 580–591.
[31] S.D. Angeli, L. Turchetti, G. Monteleone, A.A. Lemonidou, Appl. Catal. B: Environ. 181 (2016) 34–46.
[32] S. Gopalakrishnan, M.G. Faga, I. Miletto, S. Coluccia, G. Caputo, S. Sau, Appl. Catal. B: Environ. 138–139 (2013) 353–361.
[33] T. Hibino, K. Ushiki, Y. Kuwahara, Solid State Ionics 91 (1996) 69–74.
[34] S. Biswas, A. Sharma, A. Buragohain, C.V. Stayanarayana, R.N. Basu, ECS Trans. 57 (2013) 1235–1244.
[35] T. Hibino, S. Hamakawa, T. Suzuki, H. Iwahara, J. Appl. Electrochem. 24 (1994) 126–130.
[36] V. Yentekakis, Y. Jiang, S. Neophytides, S. Bebelis, C.G. Vayenas, Ionics 1 (1995) 491–498.
[37] K.H. Ryu, S. Haile, Solid State Ionics 125 (1999) 355–367.
[38] K. Katahira, Y. Kohchi, T. Shimura, H. Iwahara, Solid State Ionics 138 (2000) 91–98.
[39] S. Ricote, N. Bonanos, H.J. Wang, R. Haugsrud, Solid State Ionics 185 (2011) 11–17.
[40] S. Ricote, N. Bonanos, M.C. Marco de Lucas, G. Caboche, J. Power Sources 193 (2009) 189–193.
[41] S. Ricote, N. Bonanos, G. Caboche, Solid State Ionics 180 (2009) 990–997.
[42] V. Kyriakou, C. Athanasiou, I. Garagounis, A. Skodra, M. Stoukides, Solid State Ionics 225 (2012) 219–222.
[43] N.V. Parizotto, K.O. Rocha, S. Damyanova, F.B. Passos, D. Zanchet, C.M.P. Marques, J.M.C. Bueno, Appl. Catal. A: Gen. 330 (2007) 12–22.
[44] B.S. Liu, C.T. Au, Appl. Catal. A: Gen. 244 (2003) 181–195.
[45] L. Yang, S. Wang, K. Blinn, M. Liu, Z. Liu, Z. Cheng, M. Liu, Science 326 (2009) 126–129.
[46] A. de Lucas-Consuegra, A. Caravaca, P.J. Martínez, J.L. Endrino, F. Dorado, J.L. Valverde, J. Catal. 274 (2010) 251–258.